UJEAS

UNIZIK JOURNAL OF ENGINEERING AND APPLIED SCIENCES

UNIZIK Journal of Engineering and Applied Sciences 5(3), September (2025), 2744-2757
Journal homepage: https://journals.unizik.edu.ng/index.php/ujeas
PRINT ISSN: 2992-4383 || ONLINE ISSN: 2992-4391

Synthesis of clay, and iron oxide nanocomposites for the removal of anionic dye from aqueous media

Anolue, A. A, Ajemba, R. O., Okey-Onyesolu, C. F. and Nwachukwu, J.O.
Department of Chemical Engineering, Faculty of Engineering, Nnamdi Azikiwe University Awka, Anambra State.
Corresponding Author's E-mail: anoluearinze@gmail.com, ro.ajemba@unizik.edu.ng, cf.okey-onyesolu@unizik.edu.ng, jo.nwachukwu@unizik.edu.ng

Abstract
This experimental investigation was conducted to study the synthesis of a clay/iron oxide nanocomposite for the removal of anionic dyes from aqueous media. Batch adsorptive performance tests at various temperatures were evaluated at the optimum conditions of the adsorption parameters for the Clay/Fe_3O_4 nanocomposite adsorbent of pH, initial dye concentration, temperature, adsorbent dosage, and contact time. From the batch adsorption study, the optimum percentage removal of the anionic RR 198 dye for the Clay/Fe_3O_4 nanocomposite was obtained at pH 6. The novelty of this study is seen in the unique properties and high removal efficiency of the clay nanocomposite, combined with an iron oxide nanocomposite, with both magnetic and catalytic properties necessary for wastewater purification. The adsorption kinetic data were analyzed using several kinetic models, namely, the pseudo-first-order, pseudo-second-order, and Elovich equations. It was established that the adsorption data fitted well for the pseudo-second-order kinetic model, while the Langmuir isotherm was the best fit for the isotherm models. The evaluation of thermodynamic parameters such as the free energy ΔG^o, enthalpy ΔH^o, and the change of entropy ΔS^o gave negative values, indicating a feasible, exothermic, and spontaneous nature of the reaction.
Keywords: Nanocomposite, Adsorption, Aqueous media, Synthesis, Dye, Optimum percentage.

1. Introduction

Rapid progress in industrialization in the last few years has increased the discharge of pollutants into the environment (Das and Dey, 2020; Sivasubramaniam and Franks, 2016). Discarding municipal and other industrial wastes into water bodies causes water pollution (Lakshmi et al, 2020; Varjani and Upasani, 2017). Industries release non-treated and/or inadequately treated wastewater into the environment, which leads to water and soil pollution. Mostly pharmaceutical, textile, food, paper & pulp, and cosmetic industries use synthetic dyes for manufacturing processes. The dyeing procedure of the textile industry uses a massive volume of water in fixing, dyeing, and washing procedures. The dyes are soluble organic compounds, specifically those classified as direct, reactive, acidic, and basic. Dyes exhibit high solubility in water and make it more difficult to be removed by conventional procedures (Hassan and Carr, 2018).

Currently, water contamination due to the inability of textile industries to properly dispose of their wastewater is one of the major challenges that affects the whole world. Textile industries are major contributors to the global economy and environmental pollution in many countries, including China and South African estuaries (Olisah et al., 2021). Wastewater containing dyes is a major polluter of the environment, which also affects human health, as textile industries generate large amounts of highly colored wastewater containing a diverse range of persistent pollutants

(Almroth et al., 2021; Ali et al., 2022). Annually, about 7 × 107 tons of synthetic dyes are produced worldwide, with over 10,000 tons of such dyes used by textile industries (Chandanshive et al., 2020).

Textile wastewater has been found to contain a wide range of toxic dyes, heavy metals, such as mercury, chromium, cadmium, lead, and arsenic, which are required in the production of textile dye color pigments, as well as aromatic compounds. The presence of heavy metals such as mercury, chromium, cadmium, lead, and arsenic is required in the production of textile dye color pigments (Singha et al., 2021). These toxic chemicals are transported over long distances together with the wastewater. They then remain in the water and soil for long periods, posing serious health risks to living organisms and reducing soil fertility as well as the photosynthetic activity of aquatic plants, resulting in the development of anoxic conditions for aquatic fauna and flora (Dutta and Bhattacharjee, 2022). Textile dyes also degrade the esthetic quality of water bodies by increasing biochemical and chemical oxygen demand, thereby impairing photosynthesis, inhibiting plant growth, entering the food chain, providing recalcitrance and bioaccumulation, and potentially promoting toxicity, mutagenicity, and carcinogenicity (Mudhoo et al., 2020; Patil et al., 2022). Therefore, there is an urgent need to develop cost-effective and environmentally friendly treatment approaches for adequately treating dye-containing wastewater before its final disposal into the environment.

Globally, environmental scientists' focus has been on developing efficient and sustainable technologies for water and wastewater management (Masoudian et al, 2019; Ashraf et al, 2019; Ashraf and Hanafah, 2019). Some of the widely used methods include adsorption, membrane filtration, coagulation and flocculation, chemical precipitation, ion exchange, electrochemical removal, biosorption, reverse osmosis, and oxidation processes (Hanafah et al, 2018; Rybak et al, 2020). However, most of those methods involve high operational and maintenance costs. Among the techniques mentioned, the adsorption process using local biowastes is a cost-effective and efficient technique for removing toxic dyes and metal ions from wastewater (Hanafah et al, 2018). In recent years, researchers have focused on developing efficient adsorbents with high sorption performance and high reusability to eliminate contaminants from wastewater (Abdi et al, 2019). There have been many studies to find low-cost adsorbents for removing these contaminants. Among the natural adsorbents are rice husk (Shalaby et al, 2017), chitosan (Marques et al, 2018), chitosan/nanodiopside (Nasab et al, 2019), activated carbon prepared from pistachio shells/diopside (Rafiee, 2019), banana peels (Mondal and Kar, 2018), and sawdust (Banerjee et al, 2014; Esmaeili and Foroutan, 2019).

In this adsorption study, clay a natural material that is found in abundance in nature, with a very small structure with dimensions less than 2 microns (Khoury and Geosci, 2019), and iron resources which is readily available, simple to synthesize, and good magnetic property to adsorb dyes have led to the study of their usefulness as an adsorbent, (Tamjidi and Esmaeili, 2019). Therefore, this study centers on the combined synthesis of clay and iron oxide nanocomposites for the removal of anionic dye from aqueous media, which contributes to global efforts to improve the efficiency and safety of dye-contaminated wastewater treatment processes and disposal. To the best of our knowledge, very little research has been conducted on the utilisation of clay/iron oxide nanocomposites as an adsorbent for the adsorptive removal of anionic RR 198 dye from aqueous matrices, and no study has been made to explore the kinetics of the process. In addition, there have been many studies to find low-cost adsorbents for removing contaminants from wastewater before disposal, and this study has given a viable option to such low-cost, environmentally friendly adsorbents.

2.0 Materials and methods

2.1. Materials and Chemicals Used

The Anionic Reactive Red (RR) 198 dye and other chemicals such as HCl, NaOH, Ferric Chloride hexahydrate, Ferrous Chloride tetrahydrate, pH 7.0 buffer tablets, and distilled water of analytical grades were sourced from a chemical vendor at Bridge Head, Onitsha, Anambra state, Nigeria. A clay/iron nanocomposite was the adsorbent synthesized and used in the adsorption study. HCl and NaOH were used to adjust the pH of the dye solution, which was measured using a pH meter (PHS-25). Also, the decantation magnet was used to separate the clay/iron nanocomposite from the aqueous media, while the clay was sourced from Ukpo-Nnewi in Anambra state.

2.2 Methods

Chemical precipitation was used to synthesize the clay/iron oxide nanocomposite. Iron (III) and iron (II) with a molar ratio of 1:2 (2.71 g and 0.99 g, respectively) were added to 100 ml of distilled water and stirred at 50°C at a mixing rate of 300 rpm for 60 minutes, and iron oxide (Fe_3O_4) was obtained. 1 g of clay was added to the solution

and stirred again at 50°C and 500 rpm for 120 minutes. While stirring, sodium hydroxide (3 M) was added drop by drop to complete the oxidation process. After that, the composite was easily separated from the solution by simple decantation. The sample was washed several times with distilled water to fully neutralize and remove impurities. It was dried in an oven at 120°C for 15 hours.

2.3. Adsorption Study

2.3.1 Adsorbate Stock Solution Preparation

Reactive Red 198 Dye (chemical formula $C_{27}H_{18}CLN_7Na_4O_{15}S_5$, molecular weight = 968.21 g/mol; λ_{max} is 520 nm) was used as the adsorbate in this study. The stock solution was prepared by dissolving 1 g of Reactive Red 198 Dye in 1 liter of distilled water. The working solutions (200, 300, 400, 500, and 600 mg/l) were obtained by diluting with distilled water. The desired pH was obtained after mixing the required quantity of sodium hydroxide (0.1 M) and hydrochloric acid (0.1 M) solutions in the dye solution using a digital pH meter (PHS-25) (Baidya and Kumar, 2020).

2.3.2 Batch Adsorption Experiments

The effects of pH, adsorbent dosage, contaminant concentration, time, and temperature on the adsorption process were studied in batch mode using the modified procedure according to Okoye et al. (2019). The adsorption efficiencies of Clay/Fe_3O_4 nanocomposite were evaluated in aqueous solutions containing 200 mg/l each of anionic Reactive Red 198 Dye and placed on a magnetic stirrer. After setting the absorbance-concentration profile, anionic Reactive Red 198 Dye (RR 198) concentrations were measured by the spectrophotometric method at a determined λ_{max} ($\lambda_{max\text{-}RRD}$ = 520 nm) (Wang *et al*, 2015). The effect of main variables such as contaminant concentration (RRD: 200, 300, 400, 500, 600mg/l), pH (2, 4, 6, 8, 10), contact time (30 - 180 min), adsorbent dose (0.3 – 1.5 g/l), and temperature (30 - 70℃) were evaluated on the adsorption experiments.

The adsorption capacity of the contaminant at the time, t (qt (mg/g)) and equilibrium (qe (mg/g)) were also calculated by the following formula (Far *et al*., 2020; Khan *et al*., 2021):

$$qt = \frac{(Co - Ct)}{m} \quad (1)$$

$$qe = \frac{(Co - Ce)}{m} V \quad (2)$$

where C_0, C_e, and C_t (mg/l) are model contaminant concentrations at the initial and equilibrium stages, and time t, respectively. The adsorbent mass is m (g), and V (L) represents the model contaminant solution volume. The removal efficiency was calculated as follows (Wang *et al.*, 2020b):

$$\text{Removal efficiency (\%)}: \frac{(Co - Ce)}{Co} \times 100 \quad (3)$$

2.4 Effect of Operating Variables

2.4.1 Effect of pH

The effect of pH in the range of 2 - 10 (using pH meter, PHS-25) was studied with the optimum mas of the adsorbent at 0.3g, 30 to 180 min contact time, 300mg/l RR 198 dye, and temperature of 30 °C.

2.4.2 Effect of Adsorbent Dosage

The effect of the adsorbent dose was studied by varying the mass of the adsorbent at 0.3, 0.6, 0.9, 1.2, and 1.5 g, 30 to 180 min contact time, 300mg/l RR 198, and optimum pH 6, and temperature of 30 °C.

2.4.3 Effect of Concentration

The effect of concentration of RR 198 on the adsorption capacity of Clay/Fe_3O_4 Nanocomposite adsorbent at pH 6, and temperature of 30 °C was investigated at different concentrations of 200, 300, 400, 500, and 600mg/l RR 198, 0.3 g dose of the adsorbents, 30 to 180 min contact time.

2.4.4 Effect of Contact Time

The effect of time on the percentage of the RR 198 adsorbed by the Clay/Fe_3O_4 Nanocomposite was investigated. The batch-wise process was repeated for times 30, 60, 120, 150, and 180 minutes at 0.3 g sample dosage of the adsorbent and 300mg/L of the RR 198 at optimum pH 6 and at 30 °C temperature.

2.4.5 Effect of Temperature

The effect of temperature was studied on the adsorption performance of the adsorbent. The temperature is 30, 40, 50, 60, and 70℃; 0.3 g optimum dose of the adsorbent, 30 to 180 min contact time, 300 mg/l contaminant concentrations, and optimum pH 6, and temperature of 30 ºC.

2.5 Adsorption Kinetics Studies

The rate of the solute uptake was evaluated by an adsorption kinetics study. The rate at which the dye ions were adsorbed by the adsorbent was studied at different temperatures of 30, 40, and 50 ºC. At a constant pH of 6 for the Clay/Fe_3O_4 nanocomposite adsorbent, 0.9 g of the adsorbent and 300 mg/l of each of the solvents in a batch-wise experiment were carried out. At time intervals of about 30 min, about 10 ml of the solution was withdrawn. The withdrawn solution was filtered, and the concentration of the supernatant solution was measured and recorded. Pseudo first-order, pseudo second-order, and Elovich models were all employed to describe the rates of adsorption of the RR 198 by the Clay/Fe_3O_4 nanocomposite.

2.5.1 Pseudo-First Order

According to Lagergren, the pseudo-first-order kinetic model equations can be expressed as follows:

$$\frac{dqt}{dt} = k1(qe - qt) \quad (4)$$

where k_1 is the rate constant of the model, qt is the amount of solute adsorbed on the adsorbent at time t, and qe is the amount at equilibrium. Integrating and applying boundary conditions, qt = 0 at t = 0 and qt = qt at t = t, the natural logarithmic form of Eq. (4) was obtained:

$$\ln(qe - qt) = ln\, qe - k1t \quad (5)$$

Rearranging Eq. (5), the nonlinear form of the pseudo-first-order kinetic equation is stated as:

$$qt = qe(1 - e^{-k_1 t}) \quad (6)$$

2.5.2 Pseudo-Second Order

The non-linear pseudo-second order kinetic model equation is expressed as:

$$qt = \frac{k_2 q^2{}_e t}{1} + k_2 q_e t \quad (7)$$

where k_2 is the pseudo-second order rate constant (Saifuddin et al, 2019).

2.5.3 Elovich Isotherm

The equation that defines this model is based on a kinetic principle, which assumes that adsorption sites increase exponentially with adsorption; this implies a multilayer adsorption. The linear forms of the Elovich model are expressed as follows:

$$q_{e/q_m} = k_E C_e e^{\,q_e}/_{q_m} \quad (8)$$

but the linear form is expressed as follows:

$$\ln {q_e}/{C_e} = lnk_e q_m - {q_e}/{q_m} \quad (9)$$

Elovich maximum adsorption capacity and Elovich constant can be calculated from the slope and intercept of the plot of $\ln(qe/Ce)$ versus qe.

2.6 Adsorption Isotherm Studies

Different concentrations (200, 300, 400, and 500 mg/l) of anionic Reactive Red 198 dye were prepared. 0.9 g of the adsorbents were introduced into the solvent concentrations and agitated at 100 rpm, constant pH and temperatures at 30, 40, and 50 ºC, and the isotherm adsorption studies were carried out. After 90 mins, the solution was filtered, and the concentration of the supernatant solution was taken using a visible spectrophotometer, thus ascertaining the amount of the RR 198 ions adsorbed. The amount of RR 198 adsorbed by Clay/Fe_3O_4 nanocomposite adsorbent was calculated from Equation (1). The adsorption isotherms of the processes were studied using model equations, such as Langmuir, Freundlich, and Temkin equations.

2.6.1 Langmuir Isotherm

The Langmuir isotherm accounts for the surface coverage by balancing the relative rates of adsorption and desorption (dynamic equilibrium). The linear forms of the Langmuir and model are as shown in equation (10):

$$\frac{C_e}{q_e} = \frac{1}{q_{max}K_L} + \frac{C_e}{q_{max}} \quad (10)$$

In which q_{max} is the theoretical maximum adsorption capacity (mg/ g) when dye molecules cover a uniform monolayer on the surface. K_L (L/ mg) is the Langmuir coefficient that is related to the affinity of the binding site, i.e., adsorption energy (Hamid et al, 2017).

2.6.2 Freundlich Isotherm

The Freundlich model assumes the multilayer coverage of adsorbate onto the heterogeneous adsorbent surface, though the adsorption capacity is dependent on the equilibrium. The linear form of the Freundlich model is as shown in Equation (11):

$$\ln q_e = lnK_F + \frac{1}{n_F}\ln C_e \quad (11)$$

K_F and n_F are Freundlich constants, related to the capacity and strength of adsorption, respectively. $1/n_F$ is related to the extent of adsorbent surface heterogeneity (Hamzaoui et al, 2018).

2.6.3 Temkin Isotherm

The Temkin isotherm interplays between the adsorbent and the adsorbate and assumes that the absorbed heat decreases linearly with the surface coating, which is the reason for the adsorbent-adsorbate interaction. The linear equation of the Temkin isotherm is expressed according to equation (12):

$$q_{e=B_1}\ln K_T + B_1 \ln C_e \quad (12)$$

In this equation, B_1 (RT/b) is the Temkin constant, which represents the heat of absorption, and K_T is relevant to the maximum energy band (L/mg).

2.7. Adsorption Thermodynamics

To properly describe the changes during the sorption processes and to rightfully conclude on the nature of the reactions, thermodynamic adsorption parameters such as ΔGº, ΔHº, and ΔSº were investigated using equations 13 to 18.

$$\ln X_m = -\frac{\Delta H}{T} + K \quad (13)$$

$$\ln K_e = lnA - \frac{Ea}{RT} \quad (14)$$

Where $\ln X_m$ is the natural logarithm for the greatest amount adsorbed (mg/g), K is the constant of the Van't Hoff equation, R is the universal gas constant (8.314 J/mol. K), and T is the temperature in Kelvin.

$$\Delta G^\circ = -RTlnK \quad (15)$$

where $K = \frac{Q_e X_m}{C_e XV}$

$$\Delta G^\circ = \Delta H - T\Delta S^\circ \quad (16)$$

$$\Delta S^\circ = \frac{\Delta H - \Delta G^\circ}{T} \quad (17)$$

Combining equations 15 and 16 gives equation 18.

$$lnK_a = \left(\frac{\Delta S^\circ}{R}\right) - \left(\frac{\Delta H^\circ}{R}\right) \quad (18)$$

where Ka is the dependency of the equilibrium association constant (Ka = b, from Langmuir constant, L/mol), and R is the universal gas constant (8.314 J mol-1 K^{-1}). It is well known that the unit for ΔG^{o} is $Jmol^{-1}$. Since the unit for the term RT is also J mol^{-1}, the equilibrium constant K in Eq. (15) must be dimensionless (Nwachukwu et al, 2024), and T is the solution temperature.

3.0 Result and Discussion

3.1 Batch Adsorption Studies of the Operating Variables on the Adsorbent.

3.1.1 Effect of pH

The influence of pH on RR 198 Dye was performed in the range of pH 2 to 10 for the adsorbent dose = 0.3g, temperature = 30℃, and initial dye concentration = 30 mg/l, as shown in Figure 1. The optimum pH was observed to be at pH 6. The percentage removal increased from 3% to 73% for the Clay/iron oxide nanocomposite. RR 198 Dye is an anionic dye that stays negatively charged in solution. At a low pH, H^{+} ions easily form bonds with dye molecules in the adsorption sites, resulting in an increase in the dye removal efficiency. As the solution pH increases, however, fewer adsorption sites become available.

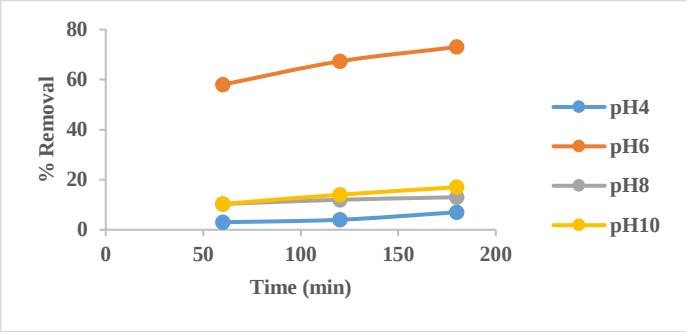

Figure 1. Influence of initial pH vs. contact Time on the adsorption efficiency of RR 198 Dye using Clay/iron oxide nanocomposites**.**

3.1.2 Effect of Adsorbent Dosage

Tests were performed with varying adsorbent doses in the scale of (0.3 – 1.5) g/20ml with the initial RR 198 Dye concentration = 30 mg/L, pH = 6, and temperature at 30 °C for the Clay/iron oxide nanocomposite. Figure 2 shows that the percentage removal improved with a reduction in doses of Clay/iron oxide nanocomposite to 0.3 g/20ml (optimum dosage), but as the dosages increased, the percentage of removal dropped significantly for the nanocomposite.

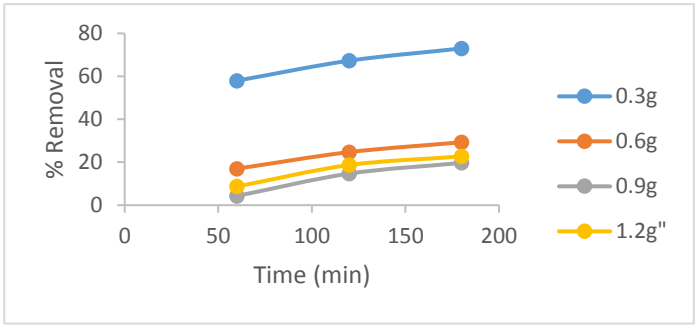

Figure 2. Influence of adsorbent dosage vs. contact Time on the adsorption efficiency of RR 198 Dye on Clay/iron oxide nanocomposites at pH 6.

3.1.3 Effects of contact time and initial concentration

From the experimental results, it is found that an average of 80% of the RR 198 Dye was adsorbed during the first 120 min. It gradually began to slow towards equilibrium in 150 min. Initially, the adsorption rate was fast because the outer surface of the sorbent had numerous sites available for adsorption. Gradually, dye molecules penetrate the adsorbent's inner pores, and the adsorption rate decreases gradually. Figure 3 shows the impact on dye adsorption

using Clay/iron oxide, with initial concentrations of 200, 300, 400, and 500 mg/L at pH 6 for nanocomposites, adsorbent dose = 0.3 g/20ml, and temperature = 30 ºC. The dye removal rates decreased as the concentration of RR 198 Dye raised from 200 to 500 mg/20ml; on the other hand, the adsorption capacity enhanced from 5.0 to 31.2 mg/g for Clay/iron oxide nanocomposite. This is because the adsorbents have a finite number of active binding sites. After a certain concentration, all such active sites were filled with dye molecules, and the adsorbents became saturated.

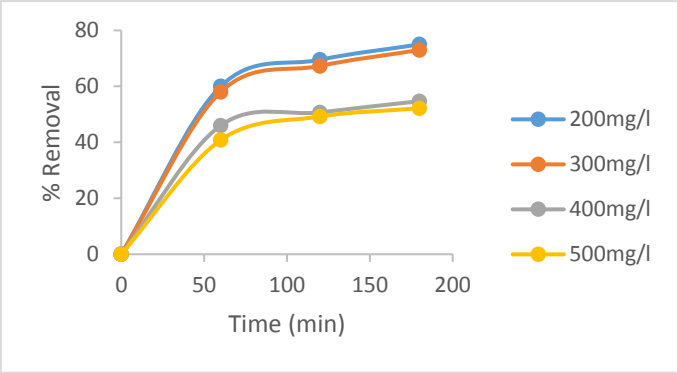

Figure 3: Influence of RR 198 Dye concentrations Vs contact time on the adsorption efficiency of RR 198 Dye for Clay/iron oxide nanocomposite.

3.1.4 Effects of Temperature

The influence of temperature on the efficiency of adsorption was studied at various temperatures in the range of 30 - 70 °C (Figure 4). The obtained results show that the RR 198 dye removal slightly decreases with increasing temperature from 30 to 70 ºC. This phenomenon indicates that the process of the removal of RR 198 by Clay/iron oxide nanocomposite is exothermic and appears to have a favourable adsorption at a lower temperature (Parisa and Rouhollah, 2020). The reason for this behavior is likely due to a decrease in the adsorptive forces between the adsorbate and adsorbent with an increase in temperature. Therefore, a temperature of 30 ºC was chosen as the optimum temperature across the three nanocomposite adsorbent.

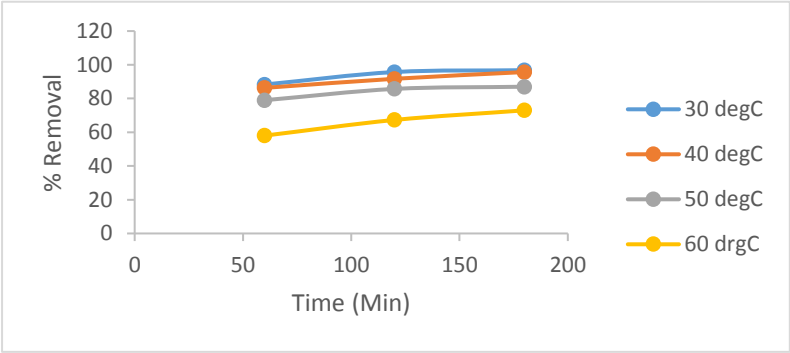

Figure 4: Influence of Temperature Vs contact time on the adsorption efficiency of RR 198 dye for Clay/iron oxide nanocomposite.

3.2 Adsorption Kinetic Studies

The kinetic data were collected experimentally by mixing 300 mg/l RR 198 dye solutions at different contact times (10–210 min) with a constant Clay/iron oxide nanocomposite dose of 0.3 g/l at temperatures of 30, 40, and 50 °C. To investigate the kinetic models, pseudo-first-order, pseudo-second-order, and Elovich models were used (Saifuddin et al, 2019). The kinetic parameters and coefficient of determination (R^2) were listed in Table 1 from the kinetic plots in Figures 5 to 7. The pseudo-second-order model fitted the experimental data better with coefficients of determination (R^2) values of 0.9995, 0.9999, and 0.9998 at the three different temperatures (30 ºC, 40 ºC, and 50 ºC) for Clay/iron oxide nanocomposite, respectively, and the calculated q_e was close to the experimental data in the pseudo-second-order model, thereby validating the model. Hence, the pseudo-second-order model described and fit the kinetic data more accurately than other kinetic models.

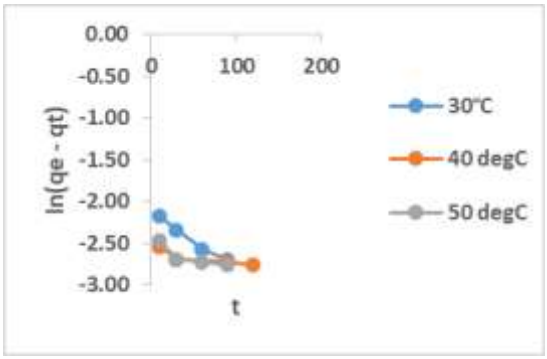

Figure 5: Pseudo-First-Order plot for RR 198 Dye on Clay/Fe_3O_4

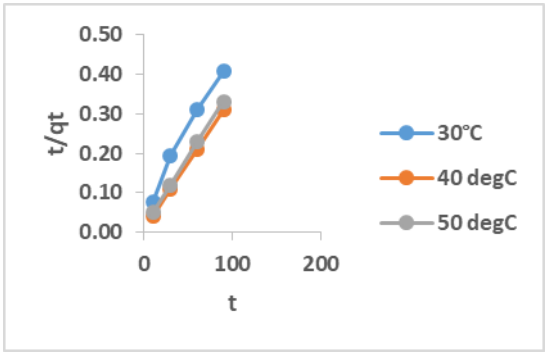

Figure 6: Pseudo-Second-Order plot for RR 198 Dye on Clay/Fe_3O_4

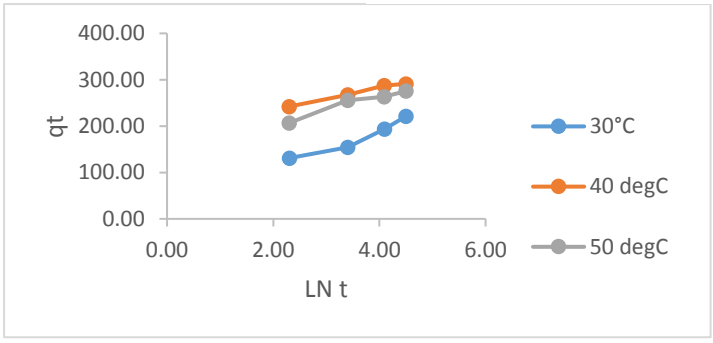

Figure 7: Elovich plot for RR 198 Dye on Clay/Fe_3O_4

Table 1: Adsorption Kinetic Parameters of Clay/Fe_3O_4 at Concentration of 300mg/l and Different Temperatures

		PFO Model			PSO Model			ELOVICH Model		
Temp (K)	**qe exp (mg/g)**	**qe Cal (mg/g)**	**K_1**	**R^2**	**qe Cal (mg/g)**	**K_2**	**R^2**	**Intercept**	**Ke**	**R^2**
303	14.47	0.1185	0.0066	0.9836	18.48	0.7139	0.9839	31.23	0.0249	0.9328
313	19.13	0.076	0.0016	0.743	131.58	0.017	0.9999	189.23	0.043	0.9869
323	17.4	0.0813	0.0032	0.7236	64.94	0.0678	0.9996	141.21	0.0328	0.945

3.3 Adsorption Isotherm

Equilibrium adsorption isotherm is very useful for the analysis and design of adsorption systems. The equilibrium adsorption experiments were carried out by batch process for different initial RR 198 dye concentrations (200 to 500 mg/l) at 30 ºC, 40 ºC, and 50 ºC. The adsorption experimental data were plotted for linear isotherm models as shown in Figures 8 to 10 for Clay/Fe_3O_4, nanocomposites, and various isotherm constants were calculated as shown in Table 2. The equilibrium adsorption data were analyzed by Langmuir, the Freundlich, and Temkin isotherm models. The coefficients of determination (R^2) showed that the obtained equilibrium data for the three temperatures were better fitted to the Langmuir isotherm model than the Freundlich and Temkin isotherm models (Table 2) for the adsorbent.

3.3.1 Langmuir Isotherm

The maximum adsorption values calculated from the Langmuir isotherm model were 29.85, 1.37, and 1.00 mg/g for Clay/Fe_3O_4 at 30 °C, 40 °C, and 50 °C, respectively. The essential characteristic of the dimensionless separation factor (R_L) values calculated as Equation (10) was in the range of 0.1311 - 0.7721, 0.0733 - 0.1651, and 0.0021 -

0.0052 for Clay/Fe_3O_4 at 20, 30, and 40 °C, respectively. The values of $0 < R_L < 1$ indicated that the adsorption of RR 198 dye was favorable at all temperatures (Hamid et al, 2017).

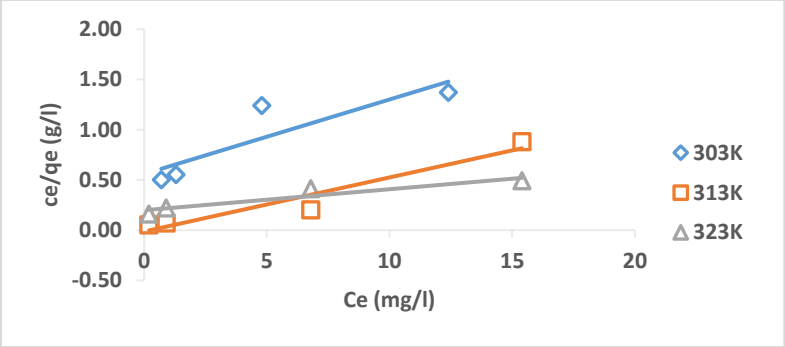

Figure 8: Langmuir isotherm plot for the adsorption of RR 198 Dye Clay/Fe_3O_4

3.3.2 Freundlich Isotherm

The Freundlich isotherm model is an empirical model that describes adsorption with a heterogeneous surface. As shown in Table 2, the value for 1/n below 1 indicated a normal Langmuir isotherm model and reflected the favorable adsorption (Hamzaoui et al, 2018).

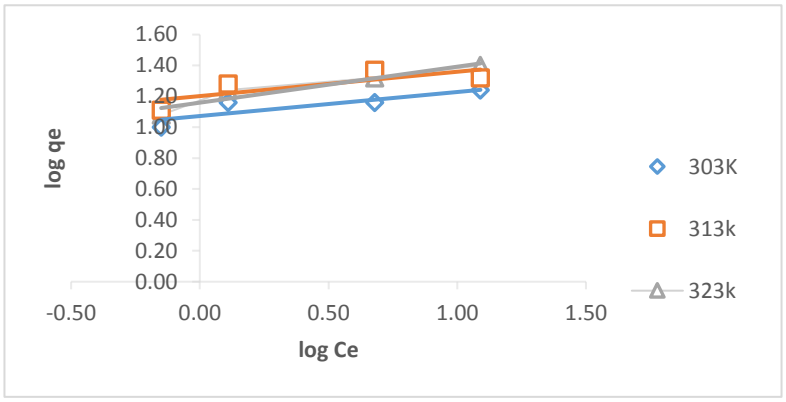

Figure 9: Freundlich isotherm plot for the adsorption of RR 198 Dye Clay/Fe_3O_4

3.3.3 Temkin Isotherm

In Table 2, the Temkin constant, A_T, can be considered a sort of adsorption potential for dye adsorption, and the calculated values were 1.0101, 0.0234, and 1.0231l/g for Clay/Fe_3O_4 at 20, 30, and 40°C, respectively. The b_T values, related to the heat of adsorption, 1.2, 0.69, and 0.65 KJ/mol for Clay/Fe_3O_4 suggest a strong interaction between RR 198 Dye molecules and adsorbent (Abedpour et al, 2020).

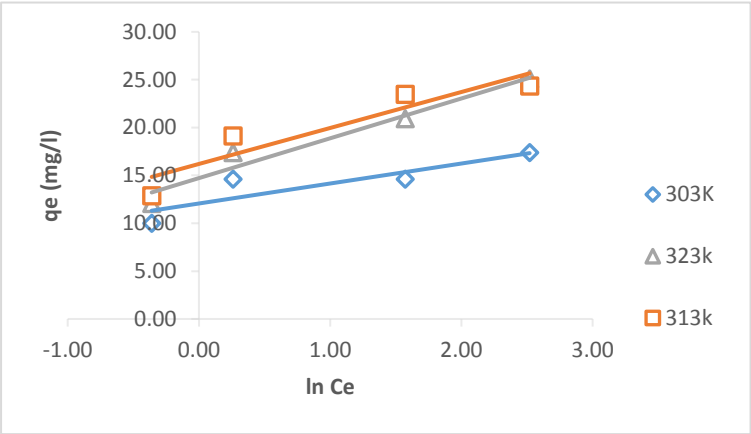

Figure 10: Temkin isotherm plot for the adsorption of RR 198 Dye Clay/Fe_3O_4

Table 2: Isotherm parameters of RR 198 Dye on Clay/Fe_3O_4 at different temperatures of 30, 40 and 50 °C (pH = 6, dose = 0.3 g, contact time = 180 min).

	Temperatures (℃)		
Isotherms	**30°C**	**40°C**	**50°C**
Langmuir Isotherm (mg/g)			
qmax (mg/g)	1.79	73.53	5.05
K_L (L/mg)	7.55	0.25	9.48
R_L	0.1311 - 0.7721	0.0733 - 0.1651	0.0021 - 0.0052
R^2	0.772	0.932	0.896
Freundlich Isotherm			
KF (L/g)	2.92	3.32	3.19
1/n	0.156	0.158	0.233
R^2	0.746	0.609	0.908
Temkin Isotherm			
B = RT/Bt	2.09	3.76	4.16
bT(KJ/mol)	1.2	0.69	0.65
A (L/g)	1.0101	0.0234	1.0231
R^2	0.778	0.956	0.861

3.4 Adsorption Thermodynamics Parameters

The adsorption thermodynamics parameters of RR 198 Dye by Clay/Fe_3O_4 nanocomposite were studied at different temperatures (30°C, 40°C, and 50°C). The equilibrium adsorption constant ($K = q_e/ C_e$) obtained at each temperature for each of the adsorbents was used for determining the free energy of adsorption (ΔG). At the initial RR 198 Dye concentrations of 200 mg/l, 300 mg/l, 400 mg/l, and 500 mg/l, the ΔG values at 30°C, 40°C, and 50°C are presented in Table 3 for Clay/Fe_3O_4 adsorbent. Then, ΔH and ΔS were determined from the intercept and slope of the straight line, respectively. ΔG values became more negative with increasing temperature, supporting that adsorption was favored with increasing temperature. The negative value of ΔG indicated the feasibility of the process and the spontaneous nature of the adsorption (Eftekhari et al, 2020). The values of ΔH and ΔS were also represented in the tables for the respective adsorbents.

Table 3: Thermodynamics Functions ΔG^o, ΔS^o, and ΔH^o of RR 198 Dye on Clay/Fe_3O_4

RR 198 Conc.				**200 Mg/l**		
T(K)	1/T(T-1)	Ln Kd = ln(qe/Ce)	Kd	ΔH^o(KJ/mol)	ΔS^o(KJ/K.mol)	ΔG^o(KJ/mol)
303	0.0033	1.3863	4	9.4455	-23.11	-34.92
313	0.0032	2.9113	18.381			-75.76
323	0.0031	1.8486	6.3509			-49.64
RR 198 Conc.				**300 Mg/l**		
T(K)	1/T(T-1)	Ln Kd = ln(qe/Ce)	Kd	ΔH^o(KJ/mol)	ΔS^o(KJ/K.mol)	ΔG^o(KJ/mol)
303	0.0033	0.5891	1.8024	16.084	-45.32	-14.84
313	0.0032	2.6891	14.7179			-6.997
323	0.0031	1.4955	4.4615			-4.016
RR 198 Conc.				**400 Mg/l**		
T(K)	1/T(T-1)	Ln Kd = ln(qe/Ce)	Kd	ΔH^o(KJ/mol)	ΔS^o(KJ/K.mol)	ΔG^o(KJ/mol)
303	0.0033	-0.2149	0.8066	18.426	-55.22	5.413
313	0.0032	1.587	4.8889			-41.302
323	0.0031	0.8896	2.4341			3.141
RR 198 Conc.				**500 Mg/l**		
T(K)	1/T(T-1)	Ln Kd = ln(qe/Ce)	Kd	ΔH^o(KJ/mol)	ΔS^o(KJ/K.mol)	ΔG^o(KJ/mol)
303	0.0033	-0.3174	0.728	16.51	-5.106	7.997
313	0.0032	0.1267	1.1351			-3.297
323	0.0031	0.7038	2.0215			-18.901

4.0. Conclusion

This study was made to study the synthesis of clay and iron oxide nanocomposites for the removal of anionic dye from aqueous media. The percentage removal of the RR 198 dye increased at pH 6 for the nanocomposite. Also, the percentage removal was optimal at 0.3 g/20ml at constant temperatures of 30 °C. It was investigated that the percentage of dye adsorbed was highest in the first 120 min. The synthesis and application of Clay/Fe_3O_4 nanoparticle for the efficient removal of anionic dye Reactive Red 198 from aqueous media in this work achieved the aim, with an optimum of 73% removal. The adsorbent was able to remove the RR 198 anionic dye from an aqueous medium to an environmentally acceptable and less toxic level before disposal, according to the National Environmental Standards and Regulations Enforcement Agency (NESREA). Also, life-threatening diseases like cancer, cholera, gene mutations, typhoid fever, and death will be hugely reduced, and lives will be preserved. It can be concluded from the results obtained that Clay/Fe_3O_4 can be used as an effective adsorbent for RR 198 anionic dye removal in aqueous media.

5.0 Recommendation

Based on the study carried out and the results obtained, the following recommendations are strongly made;

The Clay/Fe_3O_4 could be used for the same adsorptive removal of a cationic dye for future studies, since RR 198 dye is an anionic dye.

Also, the adsorbent is recommended to be used for the adsorptive removal of other contaminants like heavy metals and antibiotics from aqueous media.

In addition, apart from clay and Fe_3O_4 nanoparticles, which were synthesized and used as nanocomposite adsorbents in the process, other readily available nanoparticles could be explored for the same purpose.

Acknowledgements
I want to express my sincere gratitude to the members of the research team who contributed to the successful completion of this study. Their dedication, expertise, and commitment were instrumental in achieving our research objectives. I am also thankful to the Department of Chemical Engineering, Nnamdi Azikiwe University, Awka, for granting us access to use their laboratory throughout the period of this study.

Nomenclature
A = Temkin constant, l/g
C_e = Equilibrium concentration, mg/l;
C_o = Initial concentration, mg/l;
C_t = Concentration at time t, mg/l;
ΔG = Free energy change, kJ/mol;
ΔS = Entropy change, KJ/mol;
ΔH = Enthalpy change, KJ/mol;
RR = Reactive Red Dye
rpm = revolutions per minute
λ_{max} = maximum wavelength, nm;
R = universal gas constant (8.314 J mol-1 K^{-1});
R_L = Langmuir isotherm dimensionless separation factor

References
Abdi, J., Mahmoodi, N. M., Vossoughi, M., & Alemzadeh, I. 2019. Synthesis of magnetic metal-organic framework nanocomposite (ZIF-8@ SiO2@ MnFe2O4) as a novel adsorbent for selective dye removal from multicomponent systems. *Microporous and Mesoporous Materials*, *273*, 177-188.

Abedpour, M., Kamyab Moghadas, B. and Tamjidi, S., 2022. Equilibrium and kinetic study of simultaneous removal of Cd (II) and Ni (II) by acrylamide-based polymer as effective adsorbent: optimisation by response surface methodology (RSM). *International Journal of Environmental Analytical Chemistry*, *102*(15), pp.3524-3541.

Ahmadi, A., Foroutan, R., Esmaeili, H. and Tamjidi, S., 2020. The role of bentonite clay and bentonite clay@ MnFe2O4 composite and their physico-chemical properties on the removal of Cr (III) and Cr (VI) from aqueous media. *Environmental Science and Pollution Research*, *27*(12), pp.14044-14057.

Ali, S.S., Al-Tohamy, R., Sun, J., 2022. Performance of Meyerozyma caribbica as a novel manganese peroxidase-producing yeast inhabiting wood-feeding termite gut symbionts for azo dye decolorization and detoxification. Sci. Total Environ. 806, 150665.

Almroth, B.C., Cartine, J., Jonander, ¨ C., Karlsson, M., Langlois, J., Lindstrom, ¨ M., Lundin, J., Melander, N., Pesqueda, A., Rahmqvist, I., Renaux, J., 2021. Assessing the effects of textile leachates in fish using multiple testing methods: from gene expression to behavior. Ecotoxicol. Environ. Saf. 207, 111523.

Ashraf, M.A. and Mohd Hanafiah, M., 2019. Sustaining life on earth system through clean air, pure water, and fertile soil. *Environmental Science and Pollution Research*, *26*(14), pp.13679-13680.

Ashraf, M.A., Balkhair, K.S., Chowdhury, A.J.K. and Hanafiah, M.M., 2019. Treatment of Taman Beringin landfill leachate using the column technique. *Desalination and Water Treatment*, *149*, pp.370-387.

Banerjee, S., Chattopadhyaya, M.C., Srivastava, V. and Sharma, Y.C., 2014. Adsorption studies of methylene blue onto activated saw dust: kinetics, equilibrium, and thermodynamic studies. *Environmental Progress & Sustainable Energy*, *33*(3), pp.790-799.

Bellir, K., Bencheikh-Lehocine, M. and Meniai, A.H., 2010. Removal of methylene blue from aqueous solutions using an acid activated Algerian bentonite: equilibrium and kinetic studies. *Int Renew Energy Congr*, *2010*, pp.360-367.

Chandanshive, V., Kadam, S., Rane, N., Jeon, B.H., Jadhav, J., Govindwar, S., 2020. In situ textile wastewater treatment in high rate transpiration system furrows planted with aquatic macrophytes and floating phytobeds. Chemosphere 252, 126513.

Das, A. and Dey, A., 2020. P-Nitrophenol-Bioremediation using potent Pseudomonas strain from the textile dye industry effluent. *Journal of Environmental Chemical Engineering*, *8*(4), p.103830.

Dutta, S., Bhattacharjee, J., 2022. A comparative study between physicochemical and biological methods for effective removal of textile dye from wastewater. Development in Wastewater Treatment Research and Processes. Elsevier, pp. 1–21.

Eftekhari, M., Akrami, M., Gheibi, M., Azizi-Toupkanloo, H., Fathollahi-Fard, A.M. and Tian, G., 2020. Cadmium and copper heavy metal treatment from water resources by high-performance folic acid-graphene oxide nanocomposite adsorbent and evaluation of adsorptive mechanism using computational intelligence, isotherm, kinetic, and thermodynamic analyses. *Environmental Science and Pollution Research*, *27*(35), pp.43999-44021.

Esmaeili, H. and Foroutan, R., 2019. Adsorptive behavior of methylene blue onto sawdust of sour lemon, date palm, and eucalyptus as agricultural wastes. *Journal of Dispersion Science and Technology*. doi:10.1080/ 01932691.2018.1489828.

Far HS, Hasanzadeh M, Nashtaei MS, Rabbani M, Haji A, Hadavi Moghadam B. PPI-Dendrimer-Functionalized Magnetic Metal-Organic Framework (Fe_3O_4@MOF@PPI) with High Adsorption Capacity for Sustainable Wastewater Treatment. ACS Appl Mater Interfaces. 2020 Jun 3;12(22):25294-25303. doi: 10.1021/acsami.0c04953. Epub 2020 May 21. PMID: 32400154.

Guo S, Dan Z, Duan N, Chen G, Gao W, Zhao W 2018. Zn(II), Pb(II), and Cd(II) adsorption from aqueous solution by magnetic silica gel: preparation, characterization, and adsorption. Environ Sci Pollut Res Int 25:30938–30948.https://doi.org/10.1007/s11356-018-3050-7.

Hamid RG, Hasan P, Abdolhamid T, Kavoos D, Babak G, Vali A, Amin G 2017. Linear and nonlinear two-parameter adsorption isotherm modeling: a case-study. Int J Eng Sci. https://doi. org/10.9790/1813-0609010111.

Hamzaoui M, Bestani B, Benderdouche N (2018). The use of linear and nonlinear methods for adsorption isotherm optimization of basic green 4-dye onto sawdust-based activated carbon. J Mater Environ Sci 2508(4):1110–1118.

Hanafiah, M.M., Hashim, N.A., Ahmed, S.T. and Ashraf, M.A., 2018. Removal of chromium from aqueous solutions using a palm kernel shell adsorbent. *Desalination and Water Treatment*, *118*, pp.172-180.

Hassan, M.M. and Carr, C.M., 2018. A critical review on recent advancements of the removal of reactive dyes from dyehouse effluent by ion-exchange adsorbents. *Chemosphere*, *209*, pp.201-219.

Khan, N.A., Hasan, Z. and Jhung, S.H., 2013. Adsorptive removal of hazardous materials using metal-organic frameworks (MOFs): a review. *Journal of hazardous materials*, *244*, pp.444-456.

Khosravi, M. and Azizian, S., 2014. Adsorption of anionic dyes from aqueous solution by iron oxide nanospheres. *Journal of Industrial and Engineering Chemistry*, *20*(4), pp.2561-2567.

Khoury H.N., Arab. J. Geosci. 12, 706 (2019). doi:10.1007/s12517-019-4882-2.

Lakshmi, S., Suvedha, K., Sruthi, R., Lavanya, J., Varjani, S. and Nakkeeran, E., 2020. Hexavalent chromium sequestration from electronic waste by biomass of Aspergillus carbonarius. *Bioengineered*, *11*(1), pp.708-717.

Marques J.L. Jr, S.F. Lütke, T.S. Frantz, J.B.S. Espinelli Jr, R. Carapelli, L.A.A. Pinto and T.R. S. Cadaval Jr, 2018. Int. J. Biol. Macromol. 120, 1667 doi:10.1016/j.biomac.2018.09.135

Masoudian, N., Rajabi, M. and Ghaedi, M., 2019. Titanium oxide nanoparticles loaded onto activated carbon prepared from bio-waste watermelon rind for the efficient ultrasonic-assisted adsorption of congo red and phenol red dyes from wastewaters. *Polyhedron*, *173*, p.114105.

Mondal, N.K. and Kar, S., 2018. Potentiality of banana peel for removal of Congo red dye from aqueous solution: isotherm, kinetics and thermodynamics studies. *Applied Water Science*, *8*(6), p.157.

Mudhoo, A., Ramasamy, D.L., Bhatnagar, A., Usman, M., Sillanp¨ a¨ a, M., 2020. An analysis of the versatility and effectiveness of composts for sequestering heavy metal ions, dyes and xenobiotics from soils and aqueous milieus. Ecotoxicol. Environ. Saf. 197, 110587.

Nasab, S.G., Semnani, A., Teimouri, A., Yazd, M.J., Isfahani, T.M. and Habibollahi, S., 2019. Decolorization of crystal violet from aqueous solutions by a novel adsorbent chitosan/nanodiopside using response surface methodology and artificial neural network-genetic algorithm. *International journal of biological macromolecules*, *124*, pp.429-443.

Nwachukwu, J.O., Okoye, C. C., and Okey-Onyesolu, C. F. 2024. "Removal of Brilliant Green Dye from Simulated Wastewater Using Keratin Derived from Chicken Feathers". Journal of Materials Science Research and Reviews 7 (2):273-86. https://journaljmsrr.com/index.php/JMSRR/article/view/331.

Okoye C.C, O. D. Onukwuli & C. F. Okey-Onyesolu 2018. Predictive capability evaluation of RSM and ANN models in adsorptive treatment of crystal violet dye simulated wastewater using activated carbon prepared

from Raphiahookeri seeds, Journal of the Chinese Advanced Materials Society, 6:4, 478-496, DOI: 10.1080/22243682.2018.149753.

Olisah, C., Adams, J.B., and Rubidge, G., 2021. The state of persistent organic pollutants in South African estuaries: A review of environmental exposure and sources. Ecotoxicol. Environ. Saf. 219, 112316.

Patil, R., Zahid, M., Govindwar, S., Khandare, R., Vyavahare, G., Gurav, R., Desai, N., Pandit, S., Jadhav, J., 2022. Constructed wetland: a promising technology for the treatment of hazardous textile dyes and effluent. Development in Wastewater Treatment Research and Processes. Elsevier, pp. 173–198.

Rafiee, A., Ghanavati Nasab, S. and Teimouri, A., 2020. Synthesis and characterization of pistachio shell/nanodiopside nanocomposite and its application for removal of Crystal Violet dye from aqueous solutions using central composite design. *International Journal of Environmental Analytical Chemistry*, *100*(14), pp.1624-1649.

Rybak, M., Drzewiecka, K., Woźniak, M., Ratajczak, I. and Joniak, T., 2020. Iron-induced behavioural and biochemical responses of charophytes in consequence of phosphates coagulant addition: Threats to lake ecosystems restoration. *Chemosphere*, *254*, p.126844.

Saifuddin, M., Kim, S., Aziz, A., Kim, K.S., 2019. Mechanistic study of phosphorus adsorption onto Iron Z-A: spectroscopic and experimental approach. Appl. Sci. 9 (22), 4897.

Shalaby, N.H., Ewais, E.M., Elsaadany, R.M. and Ahmed, A., 2017. Rice husk templated water treatment sludge as low cost dye and metal adsorbent. *Egyptian journal of petroleum*, *26*(3), pp.661-668.

Singha, K., Pandit, P., Maity, S., Sharma, S.R., 2021. Harmful environmental effects for textile chemical dyeing practice. Green Chemistry for Sustainable Textiles. Woodhead Publishing, pp. 153–164

Sivasubramaniam, D. and Franks, A.E., 2016. Bioengineering microbial communities: Their potential to help, hinder and disgust. *Bioengineered*, *7*(3), pp.137-144.

Tamjidi, S. and Esmaeili, H., 2019. Chemically modified CaO/Fe3O4 nanocomposite by sodium dodecyl sulfate for Cr (III) removal from water. *Chemical Engineering & Technology*, *42*(3), pp.607-616.

Varjani, S.J. and Upasani, V.N., 2017. Critical review on biosurfactant analysis, purification and characterization using rhamnolipid as a model biosurfactant. *Bioresource technology*, *232*, pp.389-397.

Wang S, Zhang B, Li T, Li Z, Fu J 2020. Soil vanadium(V)-reducing related bacteria drive community response to vanadium pollution from a smelting plant over multiple gradients. Environ Int 138: 105630. https://doi.org/10.1016/j.envint.2020.105630

Wang, C.C., Jing, H.P., Wang, P., Gao, S.J. 2015. Seriesmetal-organic frameworks constructed from 1,10-phenanthroline and 3,3',4,4'-biphenyltetracarboxylic acid: Hydrothermal synthesis, luminescence and photocatalytic properties. *J Mol Struct* 1080: 44-51.